





## Article

# MW-Assisted Regeneration of 13X Zeolites after N<sub>2</sub>O Adsorption from Concentrated Streams: A Process Intensification

Eugenio Meloni <sup>1,\*</sup>, Marco Martino <sup>1</sup>, Mariaconcetta Pierro <sup>1</sup>, Pluton Pullumbi <sup>2</sup>, Federico Brandani <sup>2</sup> and Vincenzo Palma <sup>1</sup>

<sup>1</sup> Department of Industrial Engineering, University of Salerno, Via Giovanni Paolo II 132, 84084 Fisciano, Italy; mamartino@unisa.it (M.M.); mpierro@unisa.it (M.P.); vpalma@unisa.it (V.P.)

<sup>2</sup> Air Liquide, Paris Innovation Campus. 1, Chemin de la Porte des Loges, 78350 Les Loges en Josas, France; pluton.pullumbi@airliquide.com (P.P.); federico.brandani@airliquide.com (F.B.)

\* Correspondence: emeloni@unisa.it

**Abstract:** N<sub>2</sub>O has a global warming potential about 300 times higher than CO<sub>2</sub>, and even if its contribution to the greenhouse effect is underrated, its abatement in industrial production's tail gas has become imperative. In this work, we investigate the feasibility of the microwave (MW)-assisted regeneration of a 13X zeolite bed for N<sub>2</sub>O capture from tail gases. Several consecutive adsorption–desorption cycles were performed to verify the microwave heating effect on the zeolite's adsorption properties. The results of the experimental tests, performed at N<sub>2</sub>O concentrations of 10, 20 and 40% vol, highlighted that (i) the steps are perfectly repeatable in terms of both adsorbed and desorbed amount of N<sub>2</sub>O, meaning that the MWs did not damage the zeolite's structure, (ii) the presence of both H<sub>2</sub>O and O<sub>2</sub> in the feed stream irreversibly reduces the adsorbent capacity due to nitrites and nitrates formation, and (iii) the presence of H<sub>2</sub>O alone with N<sub>2</sub>O still reduces the adsorbent capacity of the zeolites, which can be recovered through MW-assisted regeneration at 350 °C. Moreover, the MW-assisted TSA assured an energy and purge gas saving up to 63% and 82.5%, respectively, compared to a traditional regeneration process, resulting in effective process intensification.

**Keywords:** microwaves; electrification of chemical processes; process intensification; temperature swing adsorption process; energy saving; N<sub>2</sub>O abatement



**Citation:** Meloni, E.; Martino, M.; Pierro, M.; Pullumbi, P.; Brandani, F.; Palma, V. MW-Assisted Regeneration of 13X Zeolites after N<sub>2</sub>O Adsorption from Concentrated Streams: A Process Intensification. *Energies* **2022**, *15*, 4119. <https://doi.org/10.3390/en15114119>

Academic Editors: Paitoon Tontiwachwuthikul, Zhiwu Liang and Teerawat Sema

Received: 27 April 2022

Accepted: 1 June 2022

Published: 3 June 2022

**Publisher's Note:** MDPI stays neutral with regard to jurisdictional claims in published maps and institutional affiliations.



**Copyright:** © 2022 by the authors. Licensee MDPI, Basel, Switzerland. This article is an open access article distributed under the terms and conditions of the Creative Commons Attribution (CC BY) license (<https://creativecommons.org/licenses/by/4.0/>).

## 1. Introduction

Nitrous oxide is a colorless, non-flammable and non-explosive gas. It is a minor component of the Earth's atmosphere, having an active part in the planetary nitrogen cycle, but during last decades, its concentration has undergone a rapid increase [1] with an annual growth rate of 0.2–0.3% [2]. N<sub>2</sub>O is a powerful greenhouse gas (GHG), with a global warming potential about 300 times than the CO<sub>2</sub>; however, because of its low concentration with respect to carbon dioxide, its contribution to the greenhouse effect is underrated [3]. Recently, N<sub>2</sub>O has been reported to participate in the depletion of the ozone layer in the stratosphere, too [4,5]. Since 38% or more of the N<sub>2</sub>O present in the atmosphere is the result of human activities [6] such as agriculture, chemical processes (production of adipic and nitric acid), energy industry and transportation, N<sub>2</sub>O abatement in industrial production's tail gas has become imperative. Compared to other removal methods, adsorption is considered attractive in particular for its low costs [7] and high efficiencies [8], and it is a promising way in the capture and recovery of N<sub>2</sub>O both with high and low concentrations [9]. A suitable adsorbent must combine several characteristics, including high equilibrium adsorption capacity, fast kinetics of adsorption–desorption and high selectivity for N<sub>2</sub>O. From literary studies, it has been found that activated carbons (ACs), carbon nanotubes (CNTs) and different typologies of zeolites are good adsorbents

for N<sub>2</sub>O capture. ACs have shown good adsorption properties due to their high surface area and pore volume [9,10]. CNTs have shown good chemisorption properties, resulting, especially if doped with Pd, in excellent materials for the detection of N<sub>2</sub>O but not for its removal from tail gases through desorption [11]. Regarding zeolites, they can have different structures and compositions that ensure a different capability of creating adequate nanospace and suitable microenvironments to accommodate high loading of specific molecules [12]. Among the different typologies, the zeolites ZSM-5, 5A and 13X show the best adsorption capacity toward N<sub>2</sub>O, also in the presence of water [2,7,13–17]. In particular, the 13X zeolites, besides having a well-known good adsorption capacity toward N<sub>2</sub>O, as highlighted by the previous literature studies, show also good thermal [18] and dielectric [19] properties. Representing an optimum in composition, pore volume, and channel structure [20–23], the dielectric losses are significant, and microwave heating is effective in 13X zeolites. MWs allow to directly heat the solid adsorbent [24,25], so they enable to reduce the flow rate of the purge gas and possibly the regeneration time. In this way, the desorbed gas molecules released in the core of the adsorbent bed diffuse toward the lower temperature region more promptly: since the diffusion toward the surface is the rate-determining step in the desorption process, this last is favored during microwave irradiation [26–28].

In the present work, the adsorption of N<sub>2</sub>O on 13X zeolites and the subsequent MW-assisted regeneration have been studied by using feeding streams up to 40% vol N<sub>2</sub>O. The choice of investigating concentrated streams (10, 20 and 40% vol N<sub>2</sub>O) was related to the need of removing N<sub>2</sub>O from the industrial tail gas, in case the adipic acid production reaches 30% vol. The repeatability of the adsorption–desorption cycles was verified by performing consecutive tests at the same N<sub>2</sub>O partial pressure, also aiming at verifying if MWs have any deleterious effect on the zeolites' structure. Two different types of 13X zeolites have been used, with and without iron, respectively, in order to study the influence of the iron binder in the adsorbent's structure on the whole adsorption–desorption process. Furthermore, the influence of water and its simultaneous presence with oxygen have been investigated as well by conducting both wet and dry tests. The results of this study are very promising, in particular for the optimized reactor configuration that allowed intensifying the electromagnetic field in the adsorbent bed. Compared to a traditional regeneration process, an energy saving up to 92% and a purge gas saving up to 82.5% are achieved, resulting in an effective process intensification. Finally, the COMSOL Multiphysics<sup>®</sup> software has been used to model the MW heating of the adsorbent bed together with the temperature profile inside the zeolite bed. The model realistically represented the experimental measurements of the temperature profile in the bed during desorption phase (when the MW heating is on).

## 2. Materials and Methods

### 2.1. Zeolites 13X

Two different batches of zeolites 13X were provided by Air Liquide for performing the experimental tests, which were different from each other due to the presence of iron in the binder. The two batches were identified as follows:

1. Zeolites 13X with iron in the binder: 13X-Fe;
2. Zeolites 13X without iron in the binder: 13X-noFe.

The physical properties of the provided zeolites 13X are reported in Table 1.

**Table 1.** Physical properties of the provided zeolites 13X-Fe.

Physical Property	Value
Granules average diameter (mm)	2
Density (kg/m <sup>3</sup> )	660
Void grade	0.35
Granules porosity	0.60
C <sub>p</sub> (J/kg/K)	850
Thermal conductivity (W/m/K)	0.20

## 2.2. Experimental Test Bench

The experimental test bench used for the N<sub>2</sub>O adsorption and MW-assisted desorption is shown in Figure 1.

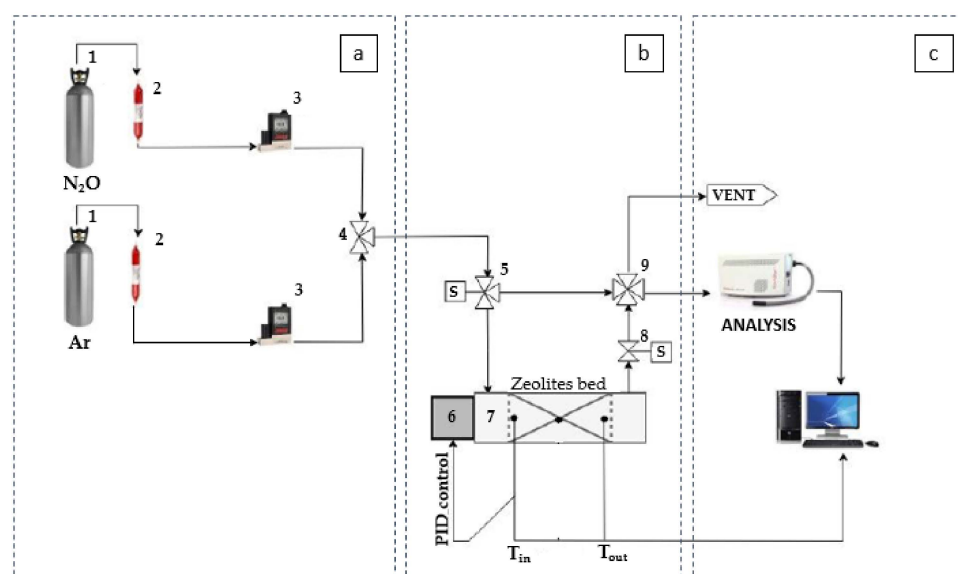


**Figure 1.** Sketch of the experimental plant. (a)—feeding section: (1) gas feeding zone; (2) moisture traps; (3) mass flow controllers; (b)—adsorption section: (4) three-way connection; (5) three-way electro valve; (6) magnetron; (7) wave guide; (8) two-way electro valve; (9) four-way connection; (c)—analysis section.

The test bench is divided in three sections, which are also shown in Figure 1:

- Gas feeding section;
- Adsorption section;
- Analysis section.

The gas feeding section sends the gas mixture to be adsorbed to the adsorber containing the 13X zeolites. The feed system provides the following lines:

- N<sub>2</sub>O feed, using two different tanks: one containing only N<sub>2</sub>O and the other containing an N<sub>2</sub>O + O<sub>2</sub> mixture (in particular 50 vol% N<sub>2</sub>O and 50 vol% O<sub>2</sub>), to investigate different features of the system, as described in the next sections;
- Argon feed;
- Moisture feed, supplied by using a bubbler.

The last feed line is used only for the wet tests (tests in which also H<sub>2</sub>O is fed).

The use of Ar as inert gas, instead of the commonly used N<sub>2</sub>, allowed avoiding mass interferences in the analysis of the gases exiting from the reactor. In fact, as detailed below, a mass spectrometer is used for this purpose.

During the adsorption phase, the mixture is composed of different partial pressures of  $N_2O$  (10, 20 or 40% vol), a same volume percentage of  $O_2$  (if present in the tank), and Ar as inert gas; instead, during the MW-assisted desorption phase, only the inert gas is fed.

To avoid any inconvenience during the adsorption phase, due to the natural moisture present in all the gas bottles, each gas line (except for the moisture one), taken from the corresponding tank, passes through a moisture trap produced by RESTEK.

For the adsorption phase, two different feed configurations have been used:

- A mixture of  $N_2O$ ,  $O_2$  and the carrier gas Ar (or only  $N_2O$  and Ar), for the dry tests;
- A mixture of  $N_2O$ ,  $O_2$ , Ar and water (or  $N_2O$ , Ar and water), for the wet tests.

For wet tests, the feed mixture passes through a bubbler, saturating itself with a certain percentage of water (equal to 1.7% vol at  $p = 1$  atm).

The flow rate of the gas mixture is controlled by using dedicated mass flow controllers.

The adsorption section consists of:

1. Stainless steel adsorber;
2. Waveguide;
3. 2.45 GHz microwaves generator system (air cooled magnetron and control features).

The adsorber configuration is very important in a MW-assisted process: if properly designed, it allows intensifying the electric field in the desired zone. In this case, the electric field is intensified where the zeolite bed is located, also minimizing MW reflection effects back to the magnetron, which can lead to its super-heating and failure. The adsorber used for the experimental tests has the same design that has been optimized during the previous reported work [24]. The optimized adsorber configuration has a restriction of the middle section (where the zeolites 13X are placed) with respect to the inlet and outlet sections in order to intensify the microwaves electric field in this zone, as shown in Figure 2. Consequently, a uniform electric field is obtained, with the result to have a better accordance between the adsorption and desorption phases.

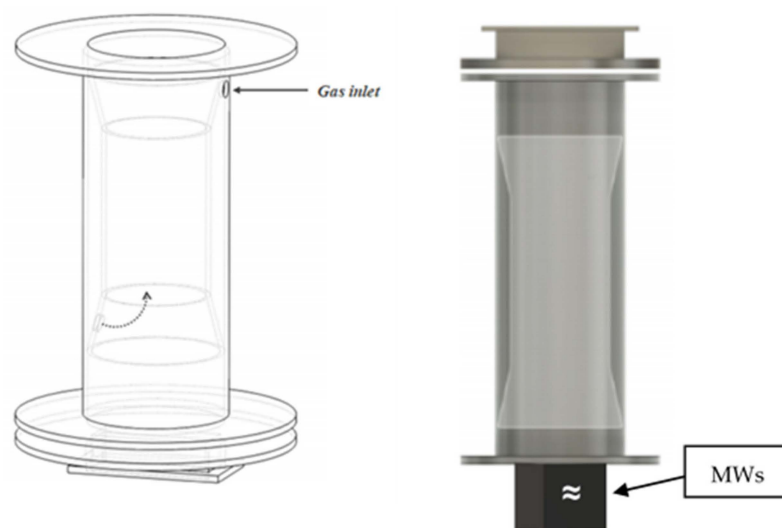


**Figure 2.** Innovative adsorber configuration.

In this configuration, the gas enters from the top, passes through the inner interspace, and then enters in the adsorber from the bottom. The internal section, in which the zeolites 13X were placed, has the diameter of 6.5 cm and is 7.5 cm long. Furthermore, to minimize leaks and prevent the gases from returning in their path and damaging the magnetron, a special rectangular slot has been designed inside the flange: in it was housed a quartz plate, transparent to microwaves, which separates the magnetron from the adsorber.

In addition, to ensure the perfect seal of the system, graphite gaskets were inserted between the flanges that connect the magnetron to the adsorber, and we used a high-temperature-resistant silicone (Motorsil) between the various junctions of the equipment.

The temperature of the zeolites bed was monitored through two specific temperature sensors insensitive to microwaves (mod. TS2 by OPTOCON), which were placed at the inlet and at the outlet of the bed. They were continuously acquired through specific software. The control of the temperature at the inlet of the zeolites bed through a PID controller allowed the exact modulation of the microwaves in order to reach the desired temperature inside the adsorber during the desorption phase.

The analysis section consists of a Pfeiffer mass spectrometer, which analyzes continuously the composition of the gas at the outlet of the adsorber.

### 2.3. Tests Processing

The experimental tests were processed in terms of amount of N<sub>2</sub>O adsorbed and desorbed, as below specified.

#### 2.3.1. Adsorbed Amount of N<sub>2</sub>O

Starting from a typical adsorption or breakthrough curve, through a mass balance, it was possible to obtain the quantity, in grams, of the adsorbed nitrous oxide:

$$dm_{N_2O} = \frac{MW}{V_m} \left[ \left( Q_{tot}^{IN} \cdot y_{N_2O}^{IN} \right) \cdot dt - \left( Q_{tot}^{OUT}(t) \cdot y_{N_2O}^{OUT}(t) \right) \cdot dt \right] \quad (1)$$

The balance equation (Equation (1)) considers that in the differential time interval  $dt$ , the mass of N<sub>2</sub>O adsorbed on the solid equals the same amount lost by the gas phase. Arranging Equation (1) and integrating between time zero and time  $t_{sat}$ , for which the complete saturation of the solid is reached, we obtain:

$$m_{N_2O} = \frac{MW}{V_m} \left[ \left( Q_{tot}^{IN} \cdot y_{N_2O}^{IN} \right) \cdot \Delta t_{tot} - \int_0^{t_{sat}} \left( Q_{tot}^{OUT}(t) \cdot y_{N_2O}^{OUT}(t) \right) \cdot dt \right] \quad (2)$$

where:

$m_{N_2O}$  is the adsorbed mass of nitrous oxide;

$MW = 44 \frac{g_{N_2O}}{mol_{N_2O}}$  is the molecular weight of the nitrous oxide;

$V_m = 22.414 \frac{L}{mol}$  is the molar volume of an ideal gas;

$Q_{tot}^{IN}$  is the volumetric flow rate of the input mixture;

$y_{N_2O}^{IN}$  is the molar fraction of nitrous oxide in the input mixture;

$t_{sat}$  is the time for which the saturation condition of the bed is reached;

$\Delta t_{tot}$  is the time interval between the switch to the gas mixture adsorber and the end of adsorption;

$y_{N_2O}^{OUT}(t)$  is the molar fraction of N<sub>2</sub>O in the output current from the adsorber, which is registered from the mass spectrometer;

$Q_{tot}^{OUT}(t)$  is the total volumetric flow rate at the exit of the adsorbent bed.

In order to compute the integral, it is necessary to consider the variation of the output flow. In fact, at the beginning, this is lower than the flow rate fed, since the N<sub>2</sub>O remains adsorbed on the bed, and it subsequently increases as the concentration of N<sub>2</sub>O in the effluent stream from the reactor increases when the bed begins to saturate.

Considering that for the tests, two different tanks have been used to feed the nitrous oxide into the adsorber, as previously described, the test processing has been carried out starting from two different mass balance equations.

#### N<sub>2</sub>O Feeding with O<sub>2</sub>

Since the system is fed with a mixture composed by argon, oxygen and nitrous oxide, the total flow rate leaving the adsorber can be calculated using the following relationship:

$$Q_{tot}^{OUT} = Q_{N_2O}^{OUT} + Q_{O_2}^{OUT} + Q_{Ar}^{OUT} \quad (3)$$

In particular, assuming that the argon is not adsorbed on the solid:

$$Q_{Ar}^{OUT} = Q_{Ar}^{IN} \quad (4)$$

Furthermore, knowing the molar fraction of  $N_2O$  and  $O_2$ , returned by the mass spectrometer, their output flow rate can be rewritten as:

$$Q_{N_2O}^{OUT} = y_{N_2O}^{OUT} \cdot Q_{tot}^{OUT} \quad (5)$$

$$Q_{O_2}^{OUT} = y_{O_2}^{OUT} \cdot Q_{tot}^{OUT} \quad (6)$$

Replacing Equations (4)–(6) in Equation (3), the following relation can be obtained:

$$Q_{tot}^{OUT} = Q_{Ar}^{IN} + Q_{tot}^{OUT} \cdot (y_{N_2O}^{OUT} + y_{O_2}^{OUT}) \quad (7)$$

So, the expression for the total flow rate, obtained from Equation (7), is a function of the incoming carrier gas flow rate and the molar fractions of oxygen and nitrous oxide:

$$Q_{tot}^{OUT} = \frac{Q_{Ar}^{IN}}{1 - (y_{N_2O}^{OUT} + y_{O_2}^{OUT})} \quad (8)$$

#### *$N_2O$ Feeding without $O_2$*

Unlike the presence of oxygen, the total flow rate leaving the adsorber can be now calculated as follows:

$$Q_{tot}^{OUT} = Q_{N_2O}^{OUT} + Q_{Ar}^{OUT} \quad (9)$$

Making the same assumption as Equation (4) and considering Equation (5), the total flow rate of Equation (9) can be rewritten:

$$Q_{tot}^{OUT} = Q_{Ar}^{IN} + Q_{tot}^{OUT} \cdot y_{N_2O}^{OUT} \quad (10)$$

Finally, the expression of the total flow rate becomes:

$$Q_{tot}^{OUT} = \frac{Q_{Ar}^{IN}}{1 - y_{N_2O}^{OUT}} \quad (11)$$

#### 2.3.2. Desorbed Amount of $N_2O$

To calculate the desorbed quantity of  $N_2O$ , the material balance applied to the compound of interest is similarly to adsorption; in this case, it is simplified as follows:

$$m_{N_2O} = \frac{MW}{V_m} \left[ \int_0^{t_f} (Q_{tot}^{OUT}(t) \cdot y_{N_2O}^{OUT}(t)) \cdot dt \right] \quad (12)$$

where

$m_{N_2O}$  is the adsorbed mass of nitrous oxide;

$MW = 44 \frac{g_{N_2O}}{mol_{N_2O}}$  is the molecular weight of the nitrous oxide;

$V_m = 22.414 \frac{L}{mol}$  is the molar volume of an ideal gas;

$Q_{tot}^{OUT}(t)$  is the total volumetric flow rate at the exit of the adsorbent bed;

$y_{N_2O}^{OUT}(t)$  is the molar fraction of nitrous oxide in the output current from the adsorber, registered from the mass spectrometer;

$t_f$  is the time for which the nitrous oxide completes the desorption process.

This calculation corresponds to the area under the desorption curve.

#### 2.4. Experimental Tests

Before carrying out the N<sub>2</sub>O adsorption and desorption tests, the adsorbent bed of zeolites was subjected to a preliminary heating process in the presence of Ar as inert gas (flow rate = 350 Ncm<sup>3</sup>/min) in order to dry the material.

The microwave heating system has been set in automatic mode, with a cyclic operation: for four seconds, it supplies the power, and for two seconds, it sets the power to zero. Once the set point value for the T<sub>in</sub> has been reached (T<sub>sp</sub> = 320 °C), the system adjusts the power in order to keep this value constant. The operating conditions used for the dry adsorption and desorption tests of N<sub>2</sub>O are shown in the following Table 2.

**Table 2.** Operating conditions of the dry mixture (with O<sub>2</sub>) in adsorption and desorption.

	Adsorption	Desorption
<b>Pressure</b>	1 atm	1 atm
<b>Flow rate</b>	1250 Ncm <sup>3</sup> /min	350 Ncm <sup>3</sup> /min
<b>Composition</b>	(i) 10% vol N <sub>2</sub> O, 10% vol O <sub>2</sub> , 80% vol Ar	100% Ar
	(ii) 20% vol N <sub>2</sub> O, 20% vol O <sub>2</sub> , 60% vol Ar	
	(iii) 40% vol N <sub>2</sub> O, 40% vol O <sub>2</sub> , 20% vol Ar	

In desorption, on the other hand, regardless of the quantity of N<sub>2</sub>O sent into the adsorber, a pressure of 1 atm and a flow rate of 350 Ncm<sup>3</sup>/min consisting of 100% Ar was used: the desorption is carried out using the microwave heating system set as previously described.

Each adsorption–desorption test has been conducted using an experimental procedure, which includes the following steps.

**Step 1—Initial stabilization of composition transient:** the gaseous mixture to be adsorbed, consisting of nitrous oxide, oxygen and argon, is sent to the bypass for a few minutes to check that the composition of the mixture was constant over time.

**Step 2—Adsorption phase:** switching the direction of the adsorption gas flow from the bypass to the adsorber, by means of a three-way solenoid valve, N<sub>2</sub>O is adsorbed by the bed of zeolites, giving rise to a typical breakthrough curve.

**Step 3—Bypass for composition change:** once the saturation condition has been reached, the composition and flow rate of the mixture are changed, together with a switch to bypass, in which the stability of the composition is checked.

**Step 4—Desorption phase:** the gas mixture is sent again into the adsorber, and then, once it reached the initial value of the partial pressure of N<sub>2</sub>O, the microwave heating system is turned on with a T<sub>sp</sub> = 320 °C; therefore, N<sub>2</sub>O will initially have an ascending and then descending trend until it reaches zero; at this point, the bed has been completely cleaned from the adsorbed N<sub>2</sub>O.

The wet tests were performed by using a flow rate of 1250 Ncm<sup>3</sup>/min, which passed through a bubbler. It was calculated that at room temperature (T = 25 °C), the water vapor pressure is  $p^{\text{sat}} = 1.713$  kPa, considering that the system pressure is constant and atmospheric, i.e.,  $p = 101.33$  kPa, the amount of H<sub>2</sub>O present in the wet stream fed into the adsorber will be 1.7% vol.

The initial adsorption stream, therefore having the features described in Table 2, will reach new values of flow rate and composition, as described in the following Table 3. The operating conditions for the desorption phase are identical to those of the dry tests.

The experimental procedure used for the adsorption–desorption wet tests is the same as that described for the dry ones.



**Table 3.** Operating conditions of the wet mixture (with O<sub>2</sub>) in adsorption and desorption.

	Adsorption	Desorption
Pressure	1 atm	1 atm
Flow rate	1271.25 Ncm <sup>3</sup> /min	350.00 Ncm <sup>3</sup> /min
Composition	39.3% vol N <sub>2</sub> O	100% Ar
	39.3% vol O <sub>2</sub>	
	1.7% vol H <sub>2</sub> O	
	19.7% vol Ar	

### 2.5. Characterization of Zeolites 13X

The zeolites after the different experimental tests were characterized by means of different physicochemical and analytical techniques. The optical analysis was performed by means of a Scanning Electron Microscope (SEM) Philips Mod.XL30, coupled to an Energy Dispersive X-ray Spectrometer (EDS) Oxford. Specific surface areas (SSA) were obtained through N<sub>2</sub> adsorption at −196 °C, by means of NOVAtouch sorptometer, applying BET method. The porosimetric characteristics of the structured samples before and after the active species deposition were evaluated by the Hg penetration technique, with a “PASCAL 140” and “PASCAL 240” (Thermo Finnigan Instruments). The structural features were evaluated with a Raman spectroscopy using an inVia Raman Microscope (Renishaw), equipped with a 514 nm Ar ion laser operating at 25 mW.

### 2.6. Modeling

The temperature profile together with the heat transfer to and from the zeolites bed was modeled by means of the finite elements software COMSOL Multiphysics<sup>®</sup> 5.4. First, the adsorber was drawn using the COMSOL CAD; the next steps were the implementation of the materials and the setting of the physics. For the materials, we implemented air in the adsorber, aluminum for the boundaries of the adsorber and zeolite for the adsorbent bed. Since the zeolite is not present in the Material Library of COMSOL, its characteristics have been introduced as a Blank Material, exploiting the physical properties of Table 1 and the dielectric properties provided by Legras et al. [29]. With regards to the physics, the MW heating system interests both the electromagnetism and the heat transfer in a porous medium. In particular, in order to predict the distribution of the electric field and the temperatures distribution when the microwave’s heating system is on, the physics “Electromagnetic Waves (Frequency domain)”, “Heat transfer in Solids” and “Heat Transfer in Fluids” were coupled in the following two Multiphysics configurations:

Electromagnetic Heating, which couples the “Electromagnetic Waves (Frequency domain)” and the “Heat Transfer in Solids” physics.

Local Thermal Non-Equilibrium, which couples the “Heat Transfer in Solids” and “Heat Transfer in Fluids” physics.

For the study of the temperature distribution in the porous medium, the Local Thermal Non-Equilibrium model was chosen, because it allows fully defining the solid, in terms of shape and dimensions of the filling components and solid volume fraction, and it allows studying the possible thermal non-equilibrium between the solid and the fluid.

The selected mesh for performing these simulations was the “physics controlled” one in order to permit the software to automatically optimize the mesh for all the domains.

For each physics, the following equations and boundary conditions have been used. *ELECTROMAGNETIC WAVE, FREQUENCY DOMAIN (EMW)*

The first equation to be presented in this physics is the wave equation. This comes from Maxwell’s equations and calculates the distribution of the electromagnetic field throughout the domain within the microwave-assisted reactor.

$$\nabla * \mu_r^{-1} * (\nabla * \mathbf{E}) - k_0^2 * \left( \epsilon_r - \frac{j * \sigma}{\omega * \epsilon_0} \right) * \mathbf{E} = 0 \quad (13)$$



The chosen port for the microwaves used in this physics is defined as “circular”, whose equation is below reported.

$$S = \frac{\int_{\partial\Omega} (E - E_1) * E_1}{\int_{\partial\Omega} E_1 * E_1} \quad (14)$$

This equation calculates the scattering “S” parameter, which is a parameter that quantifies the power not absorbed by the material absorbing the microwaves, so the power that is reflected to the source.  $E_1$  represents the input electric field vector at the gate.

The following boundary conditions have been applied for this physics.

PEC (Perfect Electric Conductor): it implies that the tangential component of the electric field is zero and is applied to metal walls; these are assumed to be ideal conductors.

$$\mathbf{n} * \mathbf{E} = 0 \quad (15)$$

Impedance Boundary Condition

$$\sqrt{\frac{\mu_0 \mu_r}{\epsilon_0 \epsilon_r - j \frac{\sigma}{\omega}}} * \mathbf{n} * \mathbf{H} + \mathbf{E} - (\mathbf{n} * \mathbf{E}) * \mathbf{n} = (\mathbf{n} * \mathbf{E}_s) * \mathbf{n} - \mathbf{E}_s \quad (16)$$

HEAT TRANSFER IN SOLID (HT)

The governing equations used in this physics are as follows.

$$\rho * C_p * \frac{\partial T}{\partial t} + \rho * C_p * \mathbf{u} * \nabla T + \nabla * \mathbf{q} = Q + Q_{ted} \quad (17)$$

$$\mathbf{q} = -k * \nabla T \quad (18)$$

Here, the appropriate boundary conditions have a thermal insulation condition.

$$-\mathbf{n} * \mathbf{q} = 0 \quad (19)$$

HEAT TRANSPORT IN FLUIDS (HT)

The governing equations used in this physics are as follows.

$$\rho * C_p * \frac{\partial T}{\partial t} + \rho * C_p * \mathbf{u} * \nabla T + \nabla * \mathbf{q} = Q + Q_p + Q_{vd} \quad (20)$$

$$\mathbf{q} = -k * \nabla T \quad (21)$$

$$\rho = \frac{p_A}{R_s * T} \text{ in Gas Ideal domain} \quad (22)$$

Here, the appropriate boundary conditions have a thermal insulation condition.

$$-\mathbf{n} * \mathbf{q} = 0 \quad (23)$$

### 3. Results and Discussion

#### 3.1. Dry Adsorption–Desorption Tests for Zeolites 13X-Fe

As an example of a complete cycle of adsorption and desorption, the curve obtained at 40% vol of  $N_2O$  is shown in Figure 3. The four steps described in the previous paragraph are shown on the graph. The general trend of the adsorption and desorption tests is similar for other values of inlet  $N_2O$  concentration.

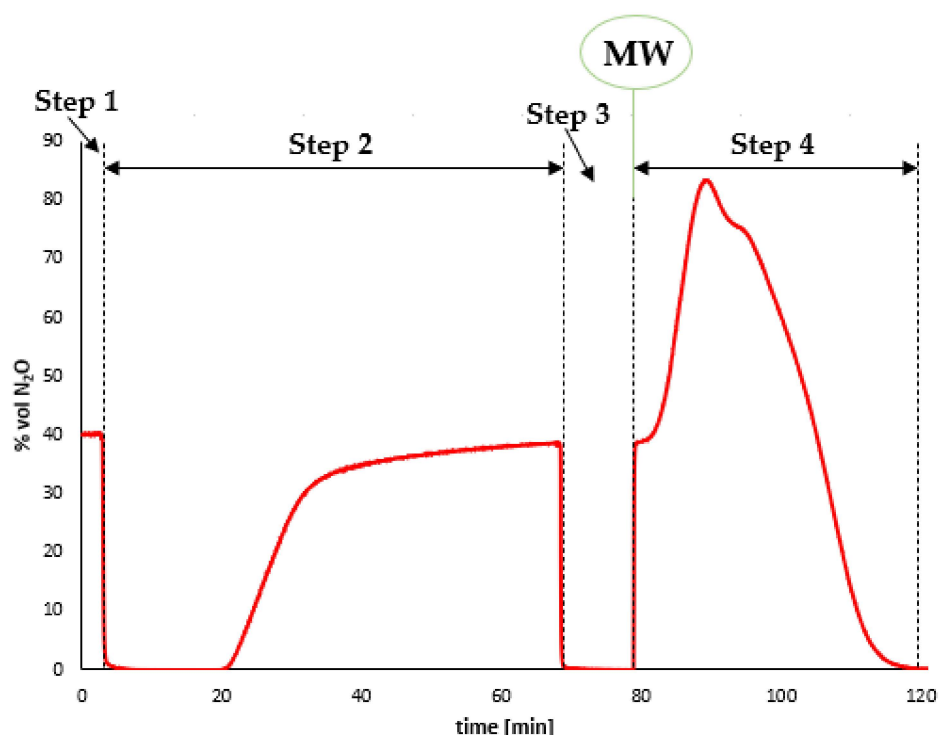


**Figure 3.** Complete adsorption and desorption cycle at 40% vol of  $N_2O$ .

More in detail, two consecutive tests were carried out for each percentage of  $N_2O$  employed in order to show the repeatability of the operation. Focusing on the breakthrough curves, the six tests are reported in the diagram below (Figure 4).

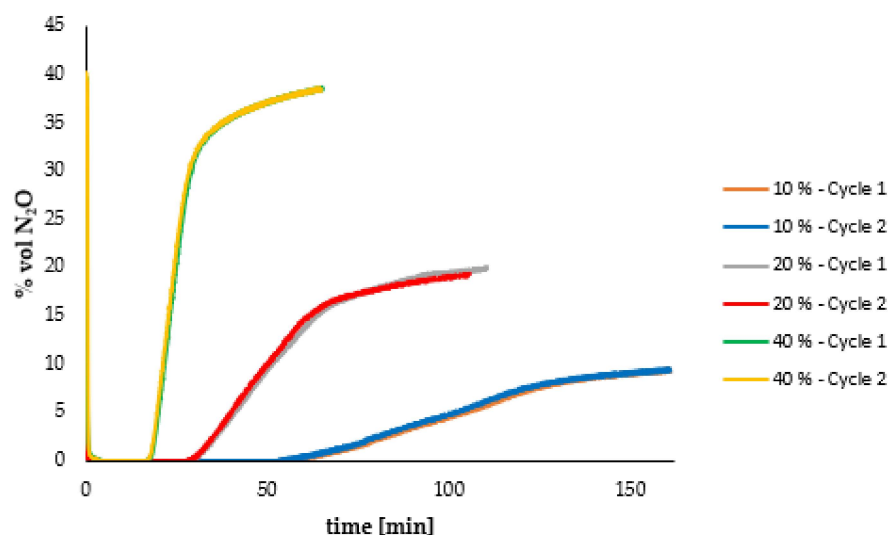


**Figure 4.** Breakthrough comparison diagram for two consecutive adsorption–desorption cycles at  $N_2O$  partial pressure of 10% vol, 20% vol, and 40% vol.

As it can be seen, for the same value of the  $N_2O$  inlet concentration, the curves for two successive tests almost superimpose. This is clear evidence of the fact that the adsorption capacity of the material has not changed. This means that the microwaves do not alter the structure of the zeolite and that the adsorbent is fully regenerated after the desorption step.

As the partial pressure of  $N_2O$  increases, in the adsorption phase, the system reaches the saturation condition in a shorter time and with a higher slope of the breakthrough curve. Moreover, the higher the initial  $N_2O$  concentration in the feed mixture is, the higher

the adsorbed mass of nitrous oxide is, as expected. The amounts of  $N_2O$  adsorbed at the three respective partial pressures (10, 20 and 40 %vol  $N_2O$ ), calculated by Equation (2), are respectively 25, 27 and 29 g; these results agree with the values provided by the adsorbent's supplier.

Comparing the desorption phase of two consecutive tests, at the same feed concentration of  $N_2O$ , it can be noted that the two curves are barely distinguishable, confirming the complete regeneration of the zeolite after each test. In Figure 5, the desorption curves for the 10% vol  $N_2O$  feed concentration case were chosen as an example.

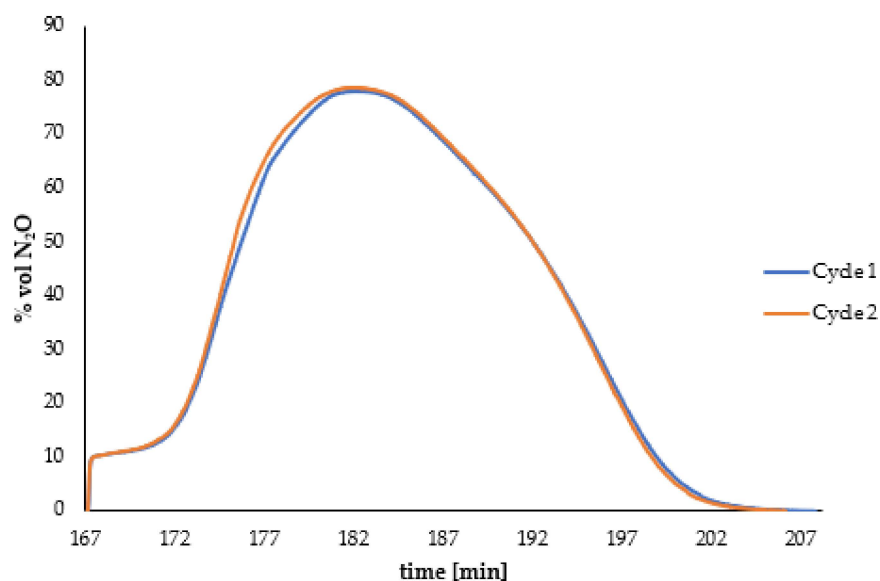


**Figure 5.** Desorption curve obtained in two consecutive cycles performed at 10% vol of  $N_2O$ .

Moreover, unless there are small experimental errors, the quantities of  $N_2O$ , respectively, adsorbed and desorbed are comparable: this is a further proof of the complete regeneration of the adsorbent bed. The desorbed amounts of  $N_2O$  were calculated using Equation (12).

### 3.2. Wet Adsorption–Desorption Tests for Zeolites 13X-Fe

After carrying out the  $N_2O$  adsorption and desorption tests described above, it was considered appropriate to evaluate the behavior of the system even in the presence of water, since a certain amount of moisture is always present in the industrial waste gases. The wet tests were carried out as previously described.

#### 3.2.1. Wet Adsorption–Desorption Tests: First Batch of Zeolite 13X-Fe

The first wet test has been carried out by using a feed mixture containing also  $O_2$ . In the presence of water, the adsorption phase of the wet 1 test has shown a behavior similar to the dry 1 test. Looking at the comparison diagram in Figure 6, a difference is found in a shorter time for which the  $N_2O$  concentration remains at zero, about 3 min less; then, the curve goes on following a trend with a certain gap with respect to the dry test but holding the same adsorption time.

The gap between the two curves reflects that a smaller amount of nitrous oxide is adsorbed: about 25.7 g versus the 29 g of the dry case. This is since water, which is a polar molecule, adsorbs more strongly than  $N_2O$ , causing a co-adsorption effect. Regarding the desorption phase, at the beginning, the same temperature ramp used for the desorption without water has been set, with which a temperature of 320 °C can be reached. After just over 50 min,  $N_2O$  ends its desorption, but needing higher temperatures to desorb water, a modification of the  $T_{sp}$  has been done. From literature studies [13], it is reported that to desorb all the chemisorbed water, it is necessary to reach temperatures above

400 °C: to avoid exceeding the maximum limit within which the zeolite retains its structural characteristics (i.e., 360 °C), the new Tsp of the MW heating was fixed to 350 °C.

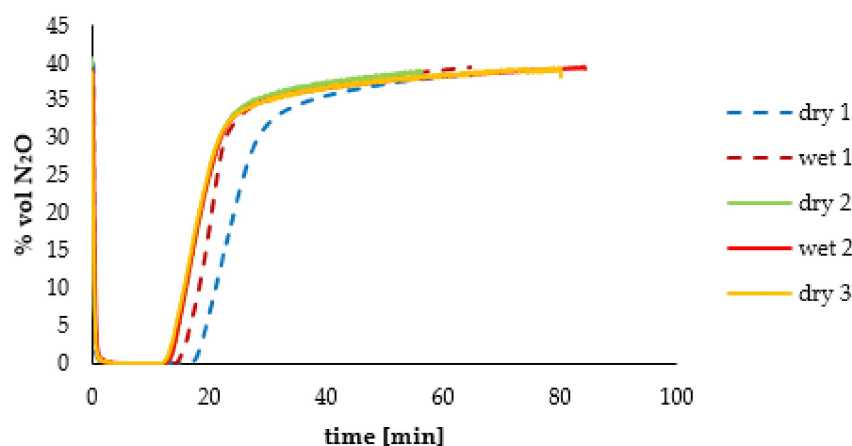


**Figure 6.** Wet and dry tests after the first dry test (dry 1).

Observing the trend of the H<sub>2</sub>O% vol and of the temperatures over time, it can be seen that a decrease in temperature corresponds to a reduction in the partial pressure of water (Figure 7), indicating a strong dependence of the percentage of outgoing water with respect to the temperature. This feature has been studied switching the control to manual mode, between the minutes 67 and 107, and then returning to the automatic mode, with the same Tsp = 350 °C. Water begins to desorb faster when the temperature is around 350 °C: its by volume percentage rises quickly until it reaches a value of just over 1%, quite stationary, which is clearly visible between 170 and 200 min. After about 24 h at the constant temperature of 350 °C, the mass spectrometer no longer detects water leaving the solid.

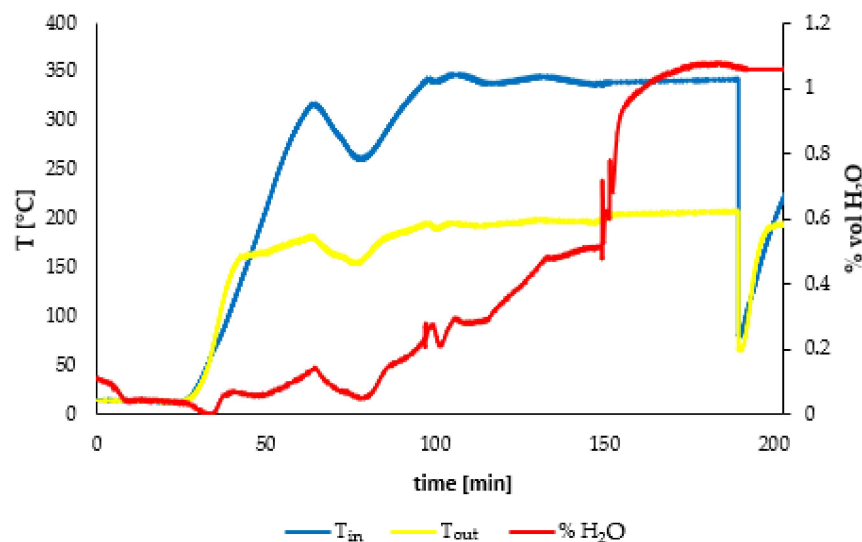


**Figure 7.** Water and temperatures trend—first wet test (with O<sub>2</sub>).

Then, several tests were carried out, alternatively both wet and dry, in order to evaluate the behavior of the zeolite after the introduction of water in the system. In particular, these tests were all conducted using a partial pressure of 40 vol% N<sub>2</sub>O (to be comparable with the test wet 1) and using the oxygen-free tank to feed the gas to be adsorbed. The conditions of both dry and wet streams were maintained at the values shown in the Tables 2 and 3, respectively, with the exception of the composition of the adsorbent mixture, which no longer contains oxygen.

The dry test after the test wet 1 produced the green breakthrough curve in Figure 6.

Moreover, in this figure, the difference between the breakthrough curves of the dry test conducted before the wet one (dry 1) and the one conducted after it (dry 2) is appreciable, with a shorter adsorption phase for the test conducted after the wet test. The calculation of the grams of adsorbed  $N_2O$  also returned this difference: while in the test dry 1, 29 g of  $N_2O$  were adsorbed, in dry 2, only 25 g of it were adsorbed, which was a result in line with the adsorbed amount of the wet 1 test.

Then, consecutive wet and dry tests were carried out, with the results shown in Figure 7. It can be noted that the breakthrough curves relating to the three wet and dry tests following the first wet one have practically the same trend, which differs from that of the first dry test: with respect to it, a reduction of about 13% in the adsorbent capacity is attested.

#### *Characterization of the First Batch of Zeolite 13X-Fe*

After obtaining the results reported in the previous paragraph, the adsorber was discharged, and a bleaching of some zeolites spheres has been observed. So, besides the reduction of the adsorbent capacity, another effect of the tests with water was a change in color. Consequently, the exhausted bed has been characterized with the previously described techniques.

Comparing the Raman spectra of the fresh and the “post  $H_2O$  adsorption–original color” samples, there are differences both in terms of change in the intensity and in the appearance of new peaks (Figure 8). From literary studies [29–34], these changes can be ascribable to the formation of nitrites and nitrates on the zeolites’ surface. In particular, the peak located at  $1045\text{ cm}^{-1}$  has been attributed to the symmetric stretching of  $NO_3^-$  [31]. Moreover, the spectrum of the white spheres of 13X zeolites (“post ads.  $H_2O$ –changed color”, Figure 8) presents the most intense band, which is located at  $510\text{ cm}^{-1}$  for the other two samples, to lower values of the Raman shift; it is justifiable with a variation of the water content in the zeolites’ structure, which led to a distortion of the framework [35].

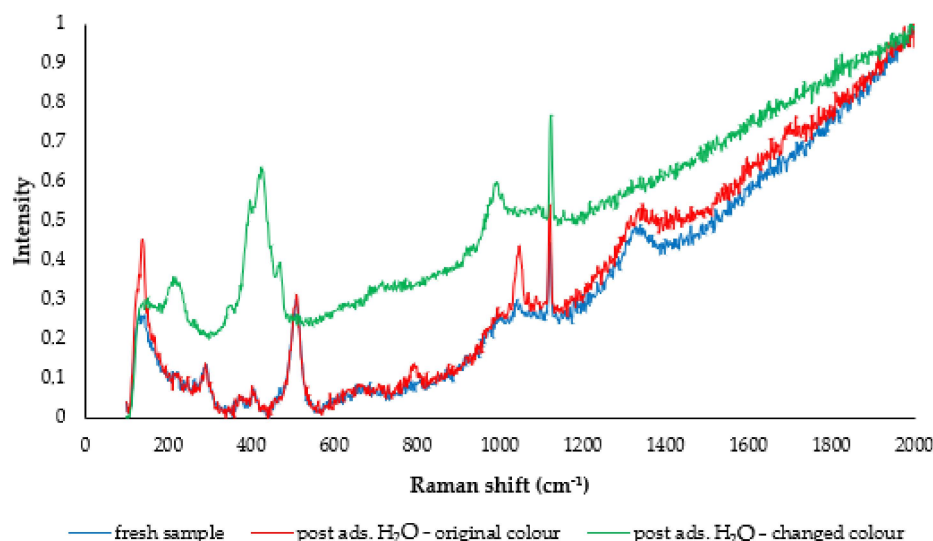


**Figure 8.** Raman spectra of fresh sample, compared with post wet adsorption 13X zeolites sample with the original and changed color.

The presence of nitrates species has been also confirmed by the thermal degradation in oxidizing conditions on the regenerated “post  $H_2O$  adsorption–original color”, which was carried out with a stream of 4%  $O_2$  and a heating rate of  $10\text{ °C/min}$ , until  $650\text{ °C}$ . By monitoring the  $m/z = 30$  in the outlet stream, index of  $NO$  and/or  $NO_2$ , a peak occurred in correspondence of a temperature of  $614\text{ °C}$ .

The changes in the zeolites' framework are confirmed even from the mercury intrusion porosimetry, whose results are retrieved in Table 4: indeed, the bleached sample shows larger pores, both in terms of average and median pore diameter, and a lower porous volume. Moreover, there are not substantial differences between fresh and post wet adsorption zeolite that has not changed color.

**Table 4.** Results of the porosimetry with Hg intrusion.

	Zeolite 13X Fresh	Zeolite 13X Post ads. H <sub>2</sub> O	Zeolite 13X Post ads. H <sub>2</sub> O (Bleached)
Average Pore Diameter (nm)	358	357	577
Median Pore Diameter (nm)	715	700	739
Total Pore Volume (mm <sup>3</sup> /g)	288	308	172

As further confirmation of the last statement, there are the results of the adsorption and desorption of nitrogen at 77 K tests for the fresh and the exhausted pink samples. The two adsorption isotherms (Figure 9) have the same shape: both are II type isotherms according to IUPAC classification [36], with small differences due to the experimental uncertainty. A same result has been obtained from the data relating to the microporous volume from the 77K–N<sub>2</sub> adsorption analysis (Table 5).

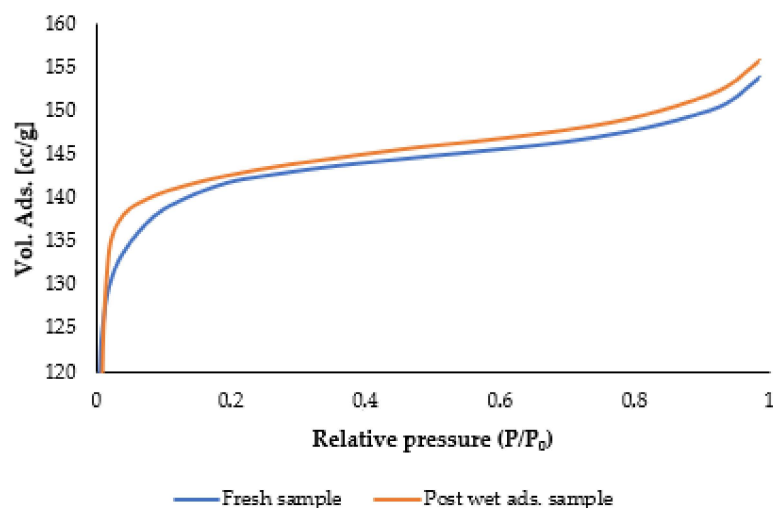


**Figure 9.** Adsorption isotherms of fresh and post wet adsorption pink samples.

**Table 5.** Results of adsorption–desorption of N<sub>2</sub> (77 K).

	Zeolite 13X-Fe Fresh	Zeolite 13X-Fe Post ads. H <sub>2</sub> O
SSA (m <sup>2</sup> /g)	381	414
Pore Radius (nm)	1.90	1.90
Micropore Volume (cm <sup>3</sup> /g)	0.015	0.013

The EDX mapping of the chemical elements respectively on the fresh sample (a) and on the bleached (b) one are displayed in Figure 10. The analysis returned a similar distribution of elements for the two samples except for iron, which was much sparser in the bleached sample. The latter is probably the reason why the zeolite has lost its initial pink color, which is due precisely to the presence of a small percentage of iron in the starting composition: the simultaneous presence of water and oxygen could bring the formation of compounds which caused the loss of iron in the metallic state.



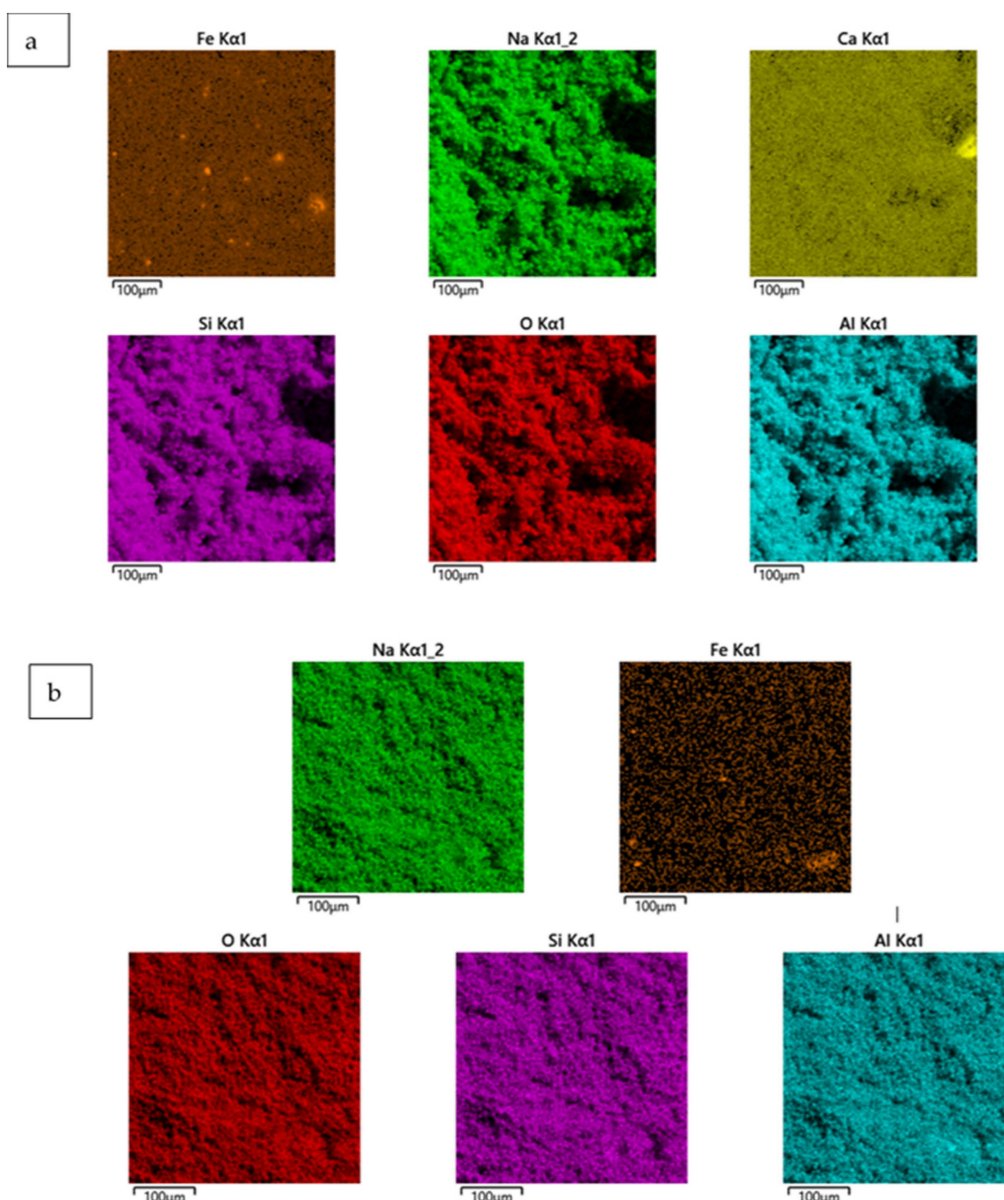


**Figure 10.** Mapping of the chemical elements—(a) Fresh sample, (b) Bleached sample.

### 3.2.2. Wet Adsorption–Desorption Tests: Second Batch of Zeolite 13X-Fe

After having discharged the adsorber and characterized the exhausted zeolites, a new batch of zeolites was introduced to conduct further tests in order to better evaluate the effect of water on the adsorption process.

Since the tests (both dry and wet) carried out after the wet 1 test all led to comparable results, using the oxygen-free tank to feed  $N_2O$ , wet and dry tests were carried out on the new batch of zeolites using the tank without oxygen. The column was loaded with 160 g of adsorbent, which corresponds to the amount used with the previous batch.

Before the first breakthrough test, the new bed has been swept with dry Ar and by heating the adsorbent using the microwave, as described previously. After evaluating the high dependence of water on temperature, through the previous tests, the Tsp has now been set at 350 °C.

In particular, one test in the presence of water (wet 3) and two in dry conditions (dry 4 and dry 5) were carried out, and the breakthrough curves obtained by these tests are shown in Figure 11 compared to the breakthrough curve of the dry 1 and wet 1 tests, too.



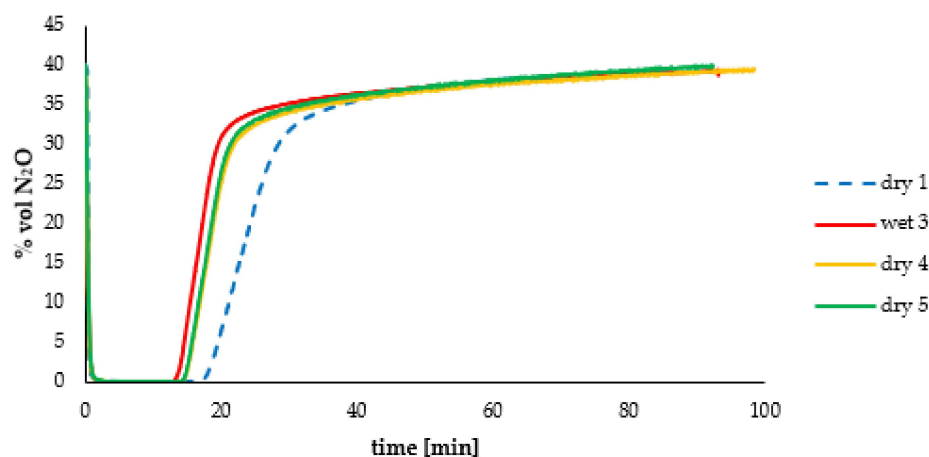


**Figure 11.** Wet and dry tests on the second zeolites batch compared to the first dry and wet tests (dry 1 and wet 1).

All the three tests show a trend of the breakthrough curve that differs from the dry 1 test and in general follows the trend of the wet 1, dry 2, wet 2 and dry 3 tests (Figure 7). However, by observing more carefully, a difference can be seen between the curves of the wet 3 and the two dry tests in terms of adsorbed  $N_2O$ , which was 25 g for the former and 27 g for the latter.

Consecutive cycles in absence of  $O_2$  were performed to verify the repeatability of the operation, which was confirmed. Therefore, the results evidenced that when the adsorbing bed is exposed to a stream also containing water, the regeneration up to 350 °C allows partially recovering the adsorbent capacity, because the system does not reach the high temperatures required to desorb all the chemisorbed water.

### 3.2.3. Wet Adsorption–Desorption Tests: Second Batch of Zeolite 13X-Fe

The results obtained from the characterizations carried out on the first batch of zeolites 13X-Fe gave the following results:

- The formation of nitrites and nitrates linked to the simultaneous presence of water and oxygen in the fed stream.
- The different distribution of iron in the sample that has become white compared to the starting one.

For this reason, the following step was used to evaluate whether the formation of nitrites and nitrates is favored by the presence of Fe in the formulation of the binder used to pelletize the zeolites. So, the adsorber was emptied again and then was filled with a batch of zeolite produced with a binder with no iron. The adsorbent bed has been activated by the same degassing procedure described in the previous paragraph. The amount of new adsorbent bed loaded into the adsorber was 160 g, which is similar to the other two previous cases. Initially, two dry tests (dry 6 and dry 7) in the presence of oxygen were conducted to have a proof of the repeatability of the operation and then have a base case of the behavior of the new adsorbent. The results of the two dry tests are shown in Figure 12 compared to the first dry test obtained from the first batch of zeolite (dry 1).

As can be seen from the overlapping of the breakthrough curves, the two dry tests are practically identical, with a quantity of adsorbed  $N_2O$ : the curves deviate from the behavior of the dry 1 test, adsorbing less nitrous oxide.

Then, a wet test (wet 4) was carried out using the operating conditions indicated in Table 3, and the results of this test are shown in the Figure 12 below.

In addition, in this case, for the wet 4 test, the presence of water and oxygen leads to a lower adsorbent capacity than the dry test with the same batch of zeolites (dry 6). These results highlighted that it is not the presence of iron in the solid to promote the formation of nitrites and nitrates, but the co-adsorption effect of water is responsible for it.

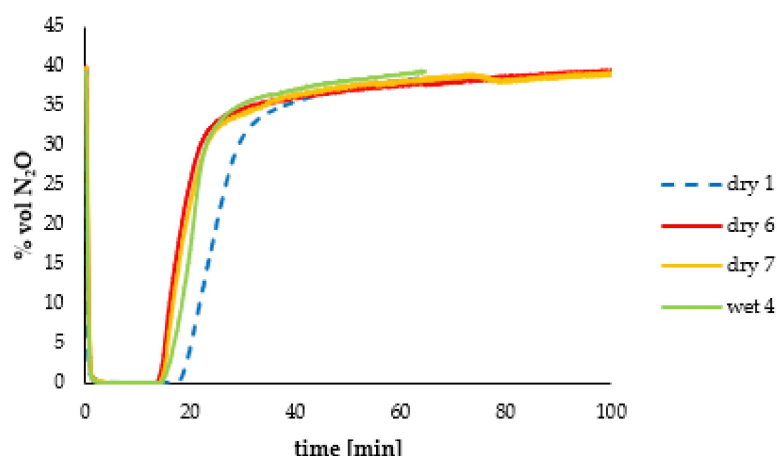


**Figure 12.** Wet and dry tests on the third zeolites batch (without Fe) compared to the first dry test (dry 1).

### 3.3. Energetic Features of the Tests

#### 3.3.1. Temperatures Trend

The  $N_2O$  concentration and the temperature profile over time for a test taken as an example (the dry1 test) is shown in Figure 13. In particular, the inlet temperature results are higher than the outlet ones for the particular path of the fresh and cold feeding gas, as described in the previous section.

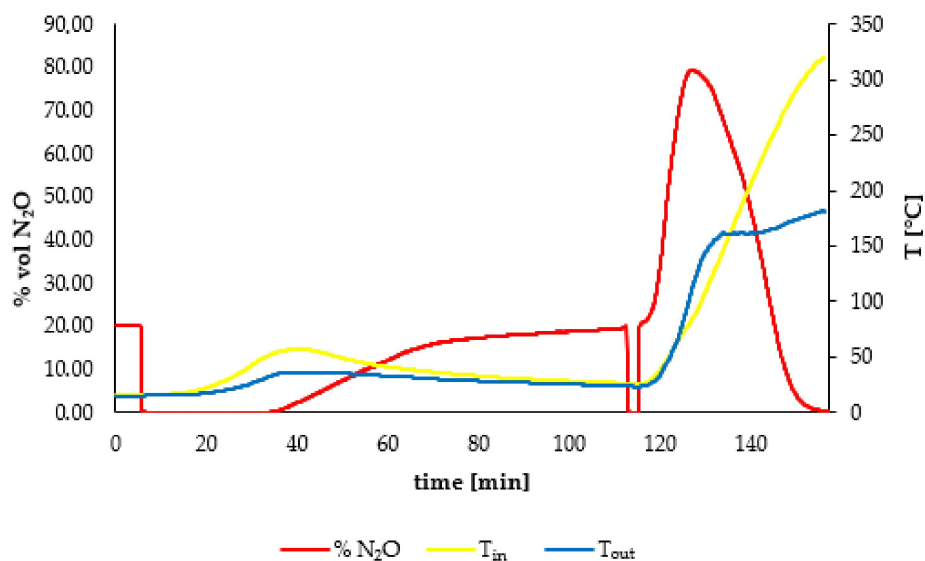


**Figure 13.** Typical temperature trend for an adsorption–desorption test of  $N_2O$  (dry 1).

At the beginning, both the temperatures at the inlet and outlet of the adsorber remain constant; when the adsorption of  $N_2O$  starts, since it is an exothermic process, the temperatures increase. Once the adsorbent reached the saturation capacity, the temperatures decrease. The adsorption step is considered finished when the inlet and outlet temperatures have the same value (about 30 °C). At this point, the adsorbent can be regenerated (in Figure 13 just after 82 min) using microwave heating. As previously described, the thermal control action through the PID controller is performed on the reactor inlet temperature ( $T_{in}$ ).

#### 3.3.2. Energy Balances

Whereas this work aims at a PI of the adsorbent's regeneration through the increase in the whole process temperature, the keystone of the work is to obtain an energy demand

comparable or lower than a traditional TSA process. Therefore, another important aspect to evaluate the performance of the heating system concerns the energy consumption related to the operation of the magnetron.

In order to compute the actual consumption of the system, it is good to remember that the magnetron supplies power in a cyclic way. More precisely, it works in the following way:

- For 2 s, a certain power is supplied.
- For 2 s, a nominal power ( $P_n$ ) is supplied that is twice the amount delivered in the previous two seconds: its value can reach 25% of the maximum power (so, 500 W).
- For 2 s  $P_n = 0$  W, namely, it nullifies its power.

This way of heating the adsorbent material aims not only to avoid a continuous supply of power, thus going toward energy saving, but also to a not too abrupt heating in order to preserve the structure of the zeolite as much as possible.

To calculate the energy consumption related to the heating system, in addition to the magnetron operating cycle, just described, the following must be considered:

- The system does not start immediately delivering all the 500 W, but in the first 8 min, the power follows the  $p$  versus  $t$  trend shown in Table 6;
- The system supplies a power of 90 W to keep the display on, so this quantity must be subtracted from all power values, and the actual supplied power  $P_{act}$  is obtained.

**Table 6.** Power trend in the initial transient phase.

$t$ (min)	$p$ (W)	$P_{act}$ (W)
0	90	0
2	230	140
4	396.5	306.5
6	462.8	372.8
8	500	410

In Table 7, for each inlet  $N_2O$  concentration, the following are reported:

- $P_{mag}$ , the power supplied by the magnetron;
- $E_{spec}$ , the specific energy, that is the energy needed to desorb a kilogram of  $N_2O$ ;
- Rec (%), the recovery percentage of  $N_2O$ , that is the ratio between the amount adsorbed and the desorbed one.

**Table 7.** Energy consumption and recovery percentage of the microwaves-assisted TSA process.

$N_2O$ (vol %)	$P_{mag}$ (W)	$E_{spec}$ (MJ/kg $N_2O$ )	Rec (%)
10	109.3	5.6	100
20	111.5	6.8	100
40	110.8	6.4	100

### 3.4. Comparison with Other TSA Processes

The energy consumption of the MW-assisted TSA process have been compared at first instance with those of two traditional TSA processes for the regeneration of 13X zeolite [37,38]. The use of MW heating allows reducing the specific energy consumption of the process and simultaneously reaching temperatures far higher (320 °C vs. 140–150 °C). Then, a comparison with another microwave-assisted TSA has been made, too. Van Schagen et al. [39] reported a specific consumption in the range of 25–50 MJ/kg $CO_2$  at a temperature of 100 °C: the adsorption tests have been conducted by also introducing water in the feed stream (30–50% RH), and the net reduction in the energy duty in our proposed technology is most likely due to the optimized configuration of the adsorber, which is an important feature in microwave heating.

In particular, in order to quantify the energy saving due to the use of microwave-assisted TSA with an optimized adsorber configuration, energy balances on our system

were carried out also by considering, respectively, the maximum regeneration temperatures of 150, 140 and 100 °C, to be comparable with the mentioned literature works [37–39]. The results have been summarized in Table 8 below.

**Table 8.** Comparison Table 1—energetic features.

Case	T <sub>max</sub> (°C)	E <sub>spec</sub> (MJ/kg <sub>ads</sub> )	Energy Saving (%)
Conventional TSA-1 [37]	150	8.8	70
Conventional TSA-2 [38]	140	6.7	63
MW-assisted TSA [39]	100	25 ÷ 50	>92

Other advantages of our system concern the low consumption of purge gas and the total recovery (100%) of N<sub>2</sub>O. In Table 9, the following data are reported for each literature work: (i) purge gas flow rates, percentage purge gas saving, as compared to our application, and the percentage recovery of adsorbed gas after each adsorption–desorption cycle.

**Table 9.** Comparison Table 2—other features.

Case	Purge Gas Flow Rate (NL/min)	Purge Gas Saving (%)	Recovery (%)
Conventional TSA-1 [37]	2	82.5	<90
Conventional TSA-2 [38]	45	99.2	≈90
MW-assisted TSA [39]	22 ÷ 30	>98.5	not defined

As evidenced by the previous comparison tables, our system allows having a great energy saving, over 63%, together with a great purge gas saving and a total recovery of the adsorbed gas, which is not achieved in the other works.

### 3.5. Modeling Results

The simulations have been carried out considering that the adsorber was swept air at a flow rate  $Q_{des}^{IN} = 350 \text{ Ncm}^3/\text{min}$ . Considering that the gas enters from the bottom of the adsorber, so it passes across the zeolite's bed section, and the gas velocity  $u_z$  has been calculated as the flowrate to section ratio, as follows:

$$u_z = \frac{Q_{des}^{IN}}{\pi \cdot \frac{D^2}{4}} \quad (24)$$

A first simulation has been carried out activating only the Electromagnetic Waves physics, in order to evaluate the distribution of the electric field into the adsorber filled with zeolites. By applying a constant MW power of 400 W, the results are shown in Figure 14.

As can be seen from Figure 14a, the electric field has a great intensity near the inlet port of the microwaves, with values around  $4 \times 10^3 \text{ V/m}$ ; then, raising along the adsorber, it decreases gradually. Looking at the volume distribution of the electric field (Figure 14a), at the adsorber's restriction and at the beginning of the zeolite's bed, the electric field undergoes an intensification, which is evident through the two lighter stripes around  $1\text{--}1.2 \times 10^3 \text{ V/m}$  and, in the zeolites bed it, as it is highlighted in the section view. Instead, focusing on the distribution of the electric field inside the zeolite's bed, the values of the electric field range from 100 to 800 V/m, as shown in Figure 14b. After this first evaluation, also, the heat transfer in solids and heat transfer in fluids physics have been coupled to the RF physic. The temperature results returned by the simulations well fitted the experimental ones: in fact, the same temperature increase in the same time interval has been obtained. The inlet temperature of the solid goes from the initial temperature of 20 °C to 44 °C after 5 min and reaches 185 °C after about 25 min (Figure 15), denoting a temperature ramp of about 9 °C/min (Figure 13).

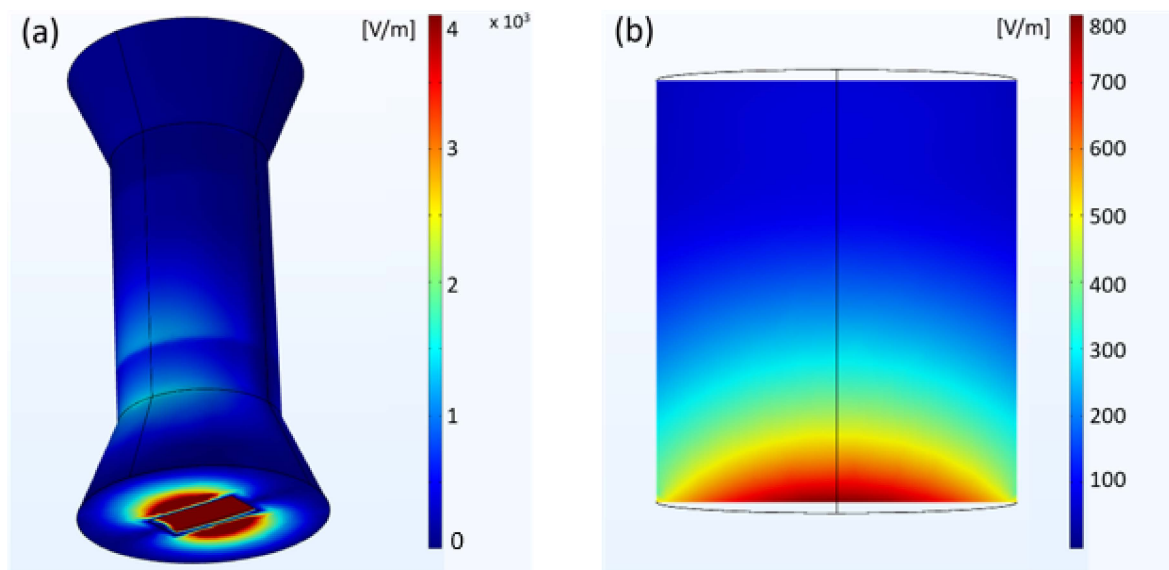


**Figure 14.** (a) Volume distribution of the electric field in the adsorber, (b) Slice distribution of the electric field in the zeolite's bed.

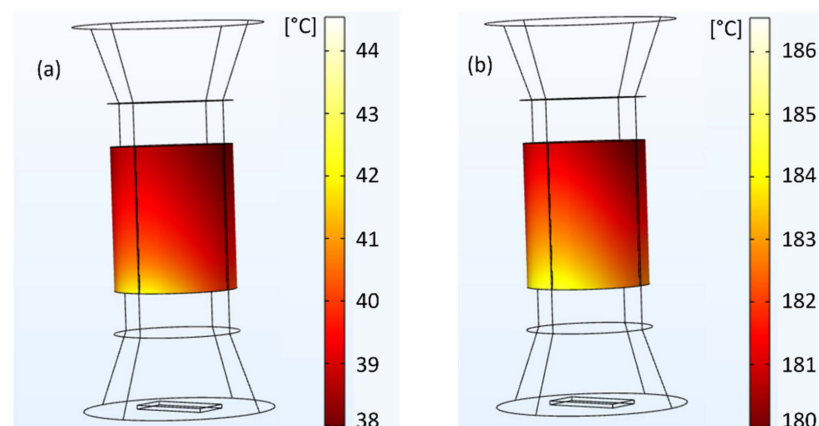


**Figure 15.** Slice distribution of the temperature in the zeolite's bed after 5 (a) and 25 (b) minutes.

#### 4. Conclusions

In this work, the influence of different parameters on the adsorption and desorption process of  $N_2O$  on 13X zeolites has been investigated, including the partial pressure of  $N_2O$  and moisture content in the feeding stream. Moreover, a process intensification has been performed, by supplying the energy in the desorption phase through a microwave heating system, thanks to the adequate dielectric properties of the 13X zeolites, which make it sensitive to electro-magnetic fields.

The conclusions of the work can be summarized as follows:

- Consecutive cycles of adsorption and MW-assisted desorption highlighted the perfect repeatability of the steps in terms of both adsorbed and desorbed amount of  $N_2O$ , meaning that the microwave radiation did not interfere with the zeolite's structure.
- The simultaneous presence of oxygen and water give rise to the formation of nitrite and nitrates and, in the bleached samples, lead to a modification in the zeolite's structure: this is visible both with a reduction in the adsorbent capacity and a loss in color by the zeolite (pink at the beginning).
- By removing oxygen from the feeding stream, the presence of water still reduces the adsorbent capacity of the adsorbent solid, which, however, manages to be recovered with the regeneration at 350 °C.

- The MW-assisted TSA has the advantage of providing heat in a volumetric way, thus ensuring an energy and purge gas saving up to 92% and 82.5%, respectively, compared to a traditional regeneration process, and a total recovery of the adsorbed N<sub>2</sub>O in a lower time.

**Author Contributions:** Conceptualization, E.M., M.M., M.P., P.P., F.B. and V.P.; methodology, E.M., M.M., M.P., P.P., F.B. and V.P.; software, E.M., M.M., M.P., P.P., F.B. and V.P.; validation, E.M., M.M., M.P., P.P., F.B. and V.P.; formal analysis, E.M., M.M., M.P., P.P., F.B. and V.P.; investigation, E.M., M.M., M.P., P.P., F.B. and V.P.; resources, E.M., M.M., M.P., P.P., F.B. and V.P.; data curation, E.M., M.M., M.P., P.P., F.B. and V.P.; writing—original draft preparation, E.M., M.M., M.P., P.P., F.B. and V.P.; writing—review and editing, E.M., M.M., M.P., P.P., F.B. and V.P.; visualization, E.M., M.M., M.P., P.P., F.B. and V.P.; supervision, E.M., M.M., M.P., P.P., F.B. and V.P.; project administration, E.M., M.M., M.P., P.P., F.B. and V.P. All authors have read and agreed to the published version of the manuscript.

**Funding:** This research received no external funding.

**Institutional Review Board Statement:** Not applicable.

**Informed Consent Statement:** Not applicable.

**Data Availability Statement:** Not applicable.

**Acknowledgments:** The authors are grateful to Paolo Tramonti for helping in the SEM-EDX analysis.

**Conflicts of Interest:** The authors declare no conflict of interest.

## References

1. Trends in Atmospheric Nitrous Oxide. National Oceanic and Atmospheric Administration/Earth System Research Laboratories. Available online: [https://gml.noaa.gov/ccgg/trends\\_n2o/](https://gml.noaa.gov/ccgg/trends_n2o/) (accessed on 22 April 2022).
2. Trinh, Q.-H.; Kim, S.H.; Mok, Y.S. Removal of dilute nitrous oxide from gas streams using a cyclic zeolite adsorption–plasma decomposition process. *Chem. Eng. J.* **2016**, *302*, 12–22. [[CrossRef](#)]
3. Heshmatifar, F.; Karimi-Sabet, J.; Khadiv-Parsi, P.; Ali Moosavian, M. The investigation of the efficient replaceable microreactor into the catalytic decomposition of N<sub>2</sub>O over Pd/anodic  $\gamma$ -Al<sub>2</sub>O<sub>3</sub>/Al. *Chem. Eng. Process. Process Intensif.* **2021**, *168*, 108555. [[CrossRef](#)]
4. Ravishankara, A.R.; Daniel, J.S.; Portmann, R.W. Nitrous oxide (N<sub>2</sub>O): The dominant ozone-depleting substance emitted in the 21st century. *Science* **2009**, *326*, 123–125. [[CrossRef](#)] [[PubMed](#)]
5. Li, Y.; Niu, S.-L.; Wang, Y.-Z.; Han, K.-H.; Zhou, W.-B.; Wang, J. Mechanism of N<sub>2</sub>O reduction by biomass gasification gas reburning. *J. Fuel Chem. Technol.* **2021**, *49*, 1435–1443. [[CrossRef](#)]
6. United States Environmental Protection Agency. *Overview of Greenhouse Gases: Nitrous Oxide Emissions*; United States Environmental Protection Agency: Washington, DC, USA, 2016.
7. Wu, T.; Shen, Y.; Feng, L.; Tang, Z.; Zhang, D. Adsorption Properties of N<sub>2</sub>O on Zeolite 5A, 13X, Activated Carbon, ZSM-5, and Silica Gel. *J. Chem. Eng. Data* **2019**, *64*, 3473–3482. [[CrossRef](#)]
8. Kloutse, F.A.; Gauthier, W.; Hourri, A.; Natarajan, S.; Benard, P.; Chahine, R. Study of competitive adsorption of the N<sub>2</sub>O-CO<sub>2</sub>-CH<sub>4</sub>-N<sub>2</sub> quaternary mixture on CuBTC. *Sep. Purif. Technol.* **2020**, *235*, 116211. [[CrossRef](#)]
9. Peng, Y.; Zhang, F.; Xu, C.; Xiao, Q.; Zhong, Y.; Zhu, W. Adsorption of Nitrous Oxide on Activated Carbons. *J. Chem. Eng. Data* **2009**, *54*, 3079–3081. [[CrossRef](#)]
10. Park, D.; Ju, Y.; Kim, J.-H.; Ahn, H.; Lee, C.-H. Equilibrium and kinetics of nitrous oxide, oxygen and nitrogen adsorption on activated carbon and carbon molecular sieve. *Sep. Purif. Technol.* **2019**, *223*, 63–80. [[CrossRef](#)]
11. Yoosefian, M. Powerful greenhouse gas nitrous oxide adsorption onto intrinsic and Pd doped Single walled carbon nanotube. *Appl. Surf. Sci.* **2017**, *392*, 225–230. [[CrossRef](#)]
12. Liu, Z.D.; Zhu, J.; Wakihara, T.; Okubo, T. Ultrafast synthesis of zeolites: Breakthrough, progress and perspective. *Inorg. Chem. Front.* **2019**, *6*, 14–31. [[CrossRef](#)]
13. Centi, G.; Generali, P.; dall’Olio, L.; Perathoner, S.; Rak, Z. Removal of N<sub>2</sub>O from industrial gaseous streams by selective adsorption over metal-exchanged zeolites. *Ind. Eng. Chem. Res.* **2000**, *39*, 131–137. [[CrossRef](#)]
14. Zhang, B.; Lu, Y.A.; He, H.; Wang, J.G.; Zhang, C.B.; Yu, Y.B.; Xue, L. Experimental and density functional theory study of the adsorption of N<sub>2</sub>O on ion-exchanged ZSM-5: Part II. The adsorption of N<sub>2</sub>O on main-group ion-exchanged ZSM-5. *J. Environ. Sci.* **2011**, *23*, 681–686. [[CrossRef](#)]
15. Guillemot, M.; Castel, B. Workplace Nitrous Oxide Sampling: Alternative Adsorbents. *Ind. Eng. Chem. Res.* **2015**, *54*, 7760–7765. [[CrossRef](#)]
16. Yamashita, K.; Liu, Z.; Iyoki, K.; Chen, C.-T.; Miyagi, S.; Yanaba, Y.; Yamauchi, Y.; Okubo, T.; Wakihara, T. Synthetic and natural MOR zeolites as high-capacity adsorbents for the removal of nitrous oxide. *Chem. Commun.* **2021**, *57*, 1312. [[CrossRef](#)]



17. Saha, D.; Deng, S. Adsorption Equilibrium, Kinetics, and Enthalpy of N<sub>2</sub>O on Zeolite 4A and 13X. *J. Chem. Eng. Data* **2010**, *55*, 3312–3317. [[CrossRef](#)]
18. Qiu, L. Thermal Properties of Framework Materials: Selected Zeolites, Clathrates and an Organic Diol. Ph.D. Thesis, National Library of Canada, Ottawa, ON, Canada, 2000.
19. Al-Mayman, S.I.; Al-Zahrani, S.M. Catalytic Cracking of Gas-Oils in Electromagnetic Fields: I—Dielectric Properties of Zeolitic Catalysts. *Catal. Lett.* **2002**, *78*, 331–337. [[CrossRef](#)]
20. Gracia, J.; Escuin, M.; Mallada, R.; Navascues, N.; Santamaría, J. Heating of zeolites under microwave irradiation: A density functional theory approach to the ion movements responsible of the dielectric loss in Na, K., and Ca A-Zeolites. *J. Phys. Chem. C* **2013**, *117*, 15659–15666. [[CrossRef](#)]
21. Somorjai, G.; Freund, H.-J. Properties of Zeolitic Catalysts. In *Catalysis Letters*; Springer: Berlin/Heidelberg, Germany, 2002.
22. Guo, Y.; Zhang, H.; Liu, Y. Desorption characteristics and kinetic parameters determination of molecular sieve by thermogravimetric analysis/differential thermogravimetric analysis technique. *Adsorpt. Sci. Technol.* **2018**, *36*, 1389–1404. [[CrossRef](#)]
23. Stankiewicz, A. Energy matters: Alternative sources and forms of energy for intensification of chemical and biochemical processes. *Chem. Eng. Res. Des.* **2006**, *84*, 511–521. [[CrossRef](#)]
24. Palma, V.; Barba, D.; Cortese, M.; Martino, M.; Renda, S.; Meloni, E. Microwaves and heterogeneous catalysis: A review on selected catalytic processes. *Catalysts* **2020**, *10*, 246. [[CrossRef](#)]
25. Meloni, E.; Iervolino, G.; Ruocco, C.; Renda, S.; Festa, G.; Martino, M.; Palma, V. Electrified Hydrogen Production from Methane for PEM Fuel Cells Feeding: A Review. *Energies* **2022**, *15*, 3588. [[CrossRef](#)]
26. Meloni, E.; Martino, M.; Pullumbi, P.; Brandani, F.; Palma, V. Intensification of TSA processes using a microwave-assisted regeneration step. *Chem. Eng. Process. Process. Intensif.* **2021**, *160*, 108291. [[CrossRef](#)]
27. Nelson, R.D., Jr.; Lide, D.R., Jr.; Maryott, A.A. *Selected Values of Electric Dipole Moments for Molecules in the Gas Phase. NSRDSNBS10*; National Standard Reference Data System-National Bureau of Standards: Washington, DC, USA, 1967.
28. Cherbanski, R.; Komorowska-Durka, M.; Stefanidis, G.D.; Stankiewicz, A.I. Microwave swing regeneration vs temperature swing regeneration—Comparison of desorption kinetics. *Ind. Eng. Chem. Res.* **2011**, *50*, 8632–8644. [[CrossRef](#)]
29. Legras, B.; Polaert, I.; Estel, L.; Thomas, M. Mechanisms Responsible for Dielectric Properties of Various Faujasites and Linde Type A Zeolites in the Microwave Frequency Range. *J. Phys. Chem. C* **2011**, *115*, 3090–3098. [[CrossRef](#)]
30. Kamboures, M.A.; van der Veer, W.; Gerberac, R.B.; Phillips, L.F. Raman spectra of complexes of HNO<sub>3</sub> and NO<sub>3</sub><sup>-</sup> with NO<sub>2</sub> at surfaces and with N<sub>2</sub>O<sub>4</sub> in solution. *Phys. Chem. Chem. Phys.* **2008**, *10*, 4748–4753. [[CrossRef](#)]
31. Kloprogge, J.T.; Frost, R.L. Raman microscopy study of basic aluminium nitrate. *Spectrochim. Acta Part A* **1999**, *55*, 163–169. [[CrossRef](#)]
32. Knops-Gerrits, P.P.; de Vos, D.E.; Feijen, E.J.P.; Jacobs, P.A. Raman spectroscopy on zeolites. *Microporous Mater.* **1997**, *8*, 3–17. [[CrossRef](#)]
33. Tsai, Y.-L.; Huang, E.; Li, Y.; Hung, H.-T.; Jiang, J.-H.; Liu, T.-C.; Fang, J.-N.; Chen, H.-F. Raman Spectroscopic Characteristics of Zeolite Group Minerals. *Minerals* **2021**, *11*, 167. [[CrossRef](#)]
34. Król, M.; Mozgawa, W.; Barczyk, K.; Bajda, T.; Kozanecki, M. Changes in the vibrational spectra of zeolites due to sorption of heavy metal cations. *J. Appl. Spectrosc.* **2013**, *80*, 644–650. [[CrossRef](#)]
35. Karge, H.G.; Geidel, E.; Characterization, I. *Molecular Sieves Science and Technology*; Springer: Berlin/Heidelberg, Germany, 2004; pp. 1–200.
36. Keller, J.; Staudt, R. *Gas Adsorption Equilibria: Experimental Methods and Adsorption Isotherms*; Springer: Berlin/Heidelberg, Germany, 2005.
37. Merel, J.; Clausse, M.; Meunier, F. Experimental Investigation on CO<sub>2</sub> Post-Combustion Capture by Indirect Thermal Swing Adsorption Using 13X and 5A Zeolites. *Ind. Eng. Chem. Res.* **2008**, *47*, 209–215. [[CrossRef](#)]
38. Jiang, N.; Shen, Y.; Liu, B.; Zhang, D.; Tang, Z.; Li, G.; Fu, B. CO<sub>2</sub> capture from dry flue gas by means of VPSA, TSA and TVSA. *J. CO<sub>2</sub> Util.* **2020**, *35*, 153–168. [[CrossRef](#)]
39. Van Schagen, T.N.; van der Wal, P.J.; Brilman, D.W.F. Development of a novel, through-flow microwave-based regenerator for sorbent-based direct air capture. *Chem. Eng. J. Adv.* **2022**, *9*, 100187. [[CrossRef](#)]